Heterogeneity Quantification of Electrophysiological Signal Propagation in High-Density Multielectrode Recordings

Lucía Pancorbo[1,2], Samuel Ruipérez-Campillo[1,3,4], Francisco Castells[1], José Millet[1,5]

[1]ITACA Institute, Universitat Politècnica de València, Valencia, Spain
[2]Bioengineering and Aerospatial Eng. Dept., Universidad Carlos III de Madrid, Spain
[3]School of Medicine, Stanford University, Palo Alto, California, United States
[4]Dept. of Inf. Tech. and Electrical Engineering, Swiss Federal Institute (ETH), Zurich, Switzerland
[5]CIBERCV Madrid

Abstract

This study presents a novel metric to evaluate the heterogeneity of cardiac substrate by using vector maps derived from omnipolar electrograms. This metric determines the level of disorganisation of electrical propagation having the potential to classify cardiac tissue under the catheter. We tested the methodology on propagation maps obtained from experimental recordings with and without electrical stimulation, under the assumption that the former exhibit greater heterogeneity. Results show the discriminatory behaviour of the parameter ($p < 0.001$), assigning higher values to non-stimulated maps and lower values in cases with stimulation. The clinical relevance of this paper lies in the introduction of a new metric defined on omnipolar-derived vector maps, capable of identifying and quantifying areas of disorganised electrical propagation within the heart. This parameter has the potential to make orientation-independent catheterisation procedures more efficient providing electrophysiologists with valuable information for the management of arrhythmias.

1. Introduction

Various metrics to measure the heterogeneity of cardiac signals have been proposed in the literature hitherto [1,2]. Nevertheless, none of these applies to propagation vector maps, which constitute a useful tool to identify conduction abnormalities and other regions of interest, including fibrotic or arrhythmogenic areas [3], or accessory pathways. The use of catheters to record electrograms (EGMs) enables the examination of cardiac conduction characteristics such as activation times, velocities, and directions. Indeed, the assessment of heart substrate is key for the diagnosis and treatment of cardiac arrhythmias.

The study of cardiac electrophysiology involves a wide range of catheters in terms of the number and arrangement of electrodes. Lately, high-density (HD) catheters are gaining importance in the field, highlighting the Advisor HD Grid catheter, with 16 electrodes organised in a 4x4 equidistant array. Its clinical relevance lies in the high resolution of the recordings and its ability to acquire omnipolar EGMs. Despite their widespread use, unipolar and bipolar EGMs have many caveats that translate to limitations in the electrophysiology laboratory. Unipolar EGMs are sensitive to low-frequency noise and far-field, whereas bipolar signal amplitude depends on the orientation of the catheter [4]. Omnipolar EGMs overcome these challenges by providing a robust and orientation-independent representation of the intracardiac signals. This technology also allows for real-time determination of electric signal propagation, as well as the visualisation of complex arrhythmogenic tissue patterns [5].

This new technique is made possible by a grid electrode arrangement. Such configuration involves the creation of cliques -defined as four nearby electrodes- from which two perpendicular bipoles are combined to obtain an omnipolar EGM [6]. Two types of cliques have been introduced in the literature: The triangular clique uses three electrodes while the square clique uses four electrodes to create bipolar signals for computation.

In impaired tissue, the electrical propagation tends to be more disorganised than in healthy areas, where it can be considered to be locally homogeneous [7]. Thus, we hypothesise that cardiac tissue can be characterised based on the degree of disorganisation in vector maps obtained from omnipolar EGMs.

To this end, we propose a novel heterogeneity metric to quantify the disorganisation of wavefront propagation. This metric, described in the methods section, involves computing and comparing the angles of propagation in the vector map. It was tested on basal and stimulated recordings. Assuming that stimulation aligns the propagation vectors decreasing the level of heterogeneity, our hypothesis is that the proposed parameter will be able to differentiate between the two groups.

2. Materials

We have selected a set of basal and stimulated recordings at 37ºC of isolated Langendorff-perfused rabbit hearts. The signals used come from a previously published research experiment [8]. In brief, an ad-hoc multielectrode mapping catheter, consisting of 128 electrodes spaced at 1mm, was placed over the epicardium of the left ventricle. Recordings were obtained (fs: 1 kHz) with the MapTech© system according to the protocol. Stimulation was performed using the GRASS S88 system and a bipolar electrode. We selected 15 recordings of each type -basal, stimulated at 4 Hz and stimulated at 6 Hz- at separate times. Each of the three recordings was obtained in different stimulation-recovering series resulting in a sample size of 45 recordings.

3. Methods

3.1. Direction of Propagation Estimation

As previously mentioned, the omnipolar technology allows instantaneous estimation of the direction of propagation. The local electric field produced by the perpendicular bipoles constituting a clique **bx-by**, forms a loop during depolarisation. The maximum amplitude of the loop coincides with the direction of wavefront propagation and is represented by a unitary vector fixed at the centre of the clique (see fig. 1).

3.2. Angle of Propagation Matrix

The signals recorded by the central 4x4 electrode array were selected to mimic the acquisition of the Advisor HD Grid Catheter. A cross-clique configuration as proposed in [9] was implemented. Based on the definition of a clique, a 3x3 vector map is obtained representing wave propagation under the catheter. The angle of propagation θ is the one comprised between each vector and the horizontal bipole $\mathbf{b_x}$. Thus, for a given instant of time on a generalised matrix of electrodes $G(t) \in \mathbb{R}^{m \times n}$ $(\forall t = c)$, we define a matrix A containing the propagation angles for each clique as:

$$A \in \mathbb{R}^{pxq} : p = m - 1, q = n - 1 \quad (1)$$

$$\theta_{i,j} : 1 \le i \le p, 1 \le j \le q \quad (2)$$

$$A := \begin{bmatrix} \theta_{1,1} & \cdots & \theta_{1,q} \\ \vdots & \ddots & \vdots \\ \theta_{p,1} & \cdots & \theta_{p,q} \end{bmatrix} \quad (3)$$

Where m and n stand for the number of rows and columns in the G matrix, p and q represent the number of rows and columns in the matrix A, and i and j indicate the location of an element in the angle matrix (as shown in fig. 2). Accordingly, the propagation is represented by a unitary vector map with elements $\vec{u}_{i,j} = (\cos\theta_{i,j}, \sin\theta_{i,j})$.

3.3. Heterogeneity Metric Derivation

For each element in the vector map, the angular variation Δθ with each of its adjacent vectors is calculated using the geometrical definition of the scalar product. For the sake of simplicity, the angular variation between two elements will be referred to as α (An example of this procedure is illustrated in fig. 2).

$$\alpha_{n_{i,j}} = cos^{-1}\langle \vec{u}_{i,j} \cdot \vec{u}_{i+c_1,j+c_2} \rangle : 1 \le i + c_1 \le p, \; 1 \le j + c_2 \le q, n = \{1, \ldots, 9\}, c_1 = \{-1,0,1\}, c_2 = \{-1,0,1\} \quad (4)$$

The constants c_1 and c_2 are used to represent all elements adjacent to $\theta_{i,j}$ including the element itself, by adding them to i and j, respectively.

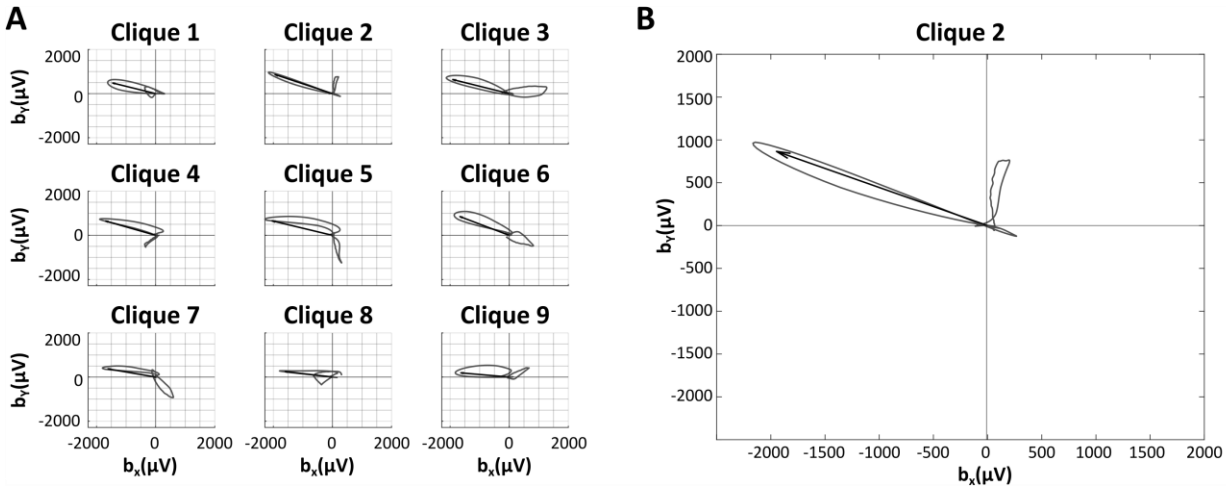

Figure 1. A. Loop traced in each clique by the corresponding bipoles. B. Magnification of the loop traced by the orthogonal bipoles of clique 2. The vector indicates the estimated direction of propagation for that clique.

Since the angular variation $\alpha_{n_{i,j}}$ can take values within the closed interval $[0, \pi]$, the summation of all variations for a given element will be upper bounded by $(\xi - 1)\pi$. The term $(\xi - 1)$ comes from the fact that one of the angular variations ($\alpha_{5_{i,j}}$ in fig. 2) is computed with itself, being null. To be exact:

$$0 \leq \alpha_{n_{i,j}} \leq \pi \Rightarrow 0 \leq \sum_{n=1}^{9} \alpha_{n_{i,j}} \leq \xi\pi \quad (5)$$

$$\alpha_{5_{i,j}} = 0, \quad \forall i,j \Rightarrow 0 \leq \sum_{n=1}^{9} \alpha_{n_{i,j}} \leq (\xi - 1)\pi \quad (6)$$

The variable ξ depends on the position of the element within the matrix of angles. Taking the value of 9, 4, or 6 depending on whether it is a central, vertex, or side element, respectively.

For each element of the matrix, a heterogeneity coefficient $v_{i,j}$ is calculated by summing all the angular variations and dividing by the upper limit to obtain a value between 0 and 1:

$$v_{i,j} = \frac{\sum_{n=1}^{9} \alpha_{n_{i,j}}}{(\xi - 1)\pi} \quad : \; 0 \leq v_{i,j} \leq 1 \quad (7)$$

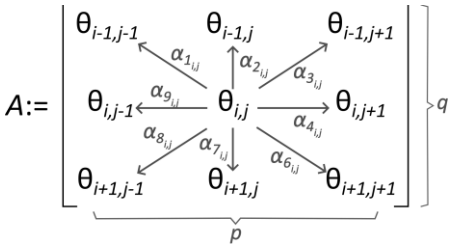

Figure 2. Angular variations for a central element $\theta_{i,j}$.

The resulting value is then assigned to the corresponding propagation map element representing how different that vector is from its contiguous elements (see fig. 3). Finally, all coefficients are averaged to obtain the global heterogeneity value *H*:

$$H = \frac{\sum_{i=1}^{p} \sum_{j=1}^{q} v_{i,j}}{p \times q} \quad : \; 0 \leq H < 1 \quad (8)$$

3.4. Statistical Analysis

To evaluate the performance of the parameter, it was applied to basal and stimulated recordings. Its potential to quantify heterogeneity of propagation relies on its ability to distinguish between populations according to the stimulation. The *H* values (see fig. 4a) were analysed for significant differences using a Kruskal-Wallis test with a post-hoc Dunn's pairwise test with the Bonferroni correction (1% significance level). These non-parametric options were chosen due to the non-normal distribution of the data, confirmed by the Saphiro-Wilk test.

4. Results

Examples of heterogeneity maps and the corresponding vector map from which they were derived are shown in fig. 3. Both recordings were taken at 37ºC. One with applied stimulation (fig. 3.a) and the other without stimulation (fig. 3.b).

Significant differences are found between the compared groups according to the Kruskal-Wallis test ($p<0.01$). Thus, a pairwise comparison is performed using Dunn's test. A significant distinction is observed when comparing the results from the basal group to those of the stimulated group, however, no meaningful difference was found between the groups that received stimulation at 4 and 6 Hz (see table 1).

Table 1. P-values of Dunn's Test Comparing *H* values according to Stimulation Type

Comparison	p-value uncorrected	p-value corrected
Basal - Stim. 4 Hz	9.25e-07*	2.77e-06*
Basal - Stim. 6 Hz	1.12e-05*	3.36e-05*
Stim. 4 Hz - Stim. 6 Hz	0.61	1

* p-values < 0.01, Basal = Non-stimulated, Stim. = Stimulated

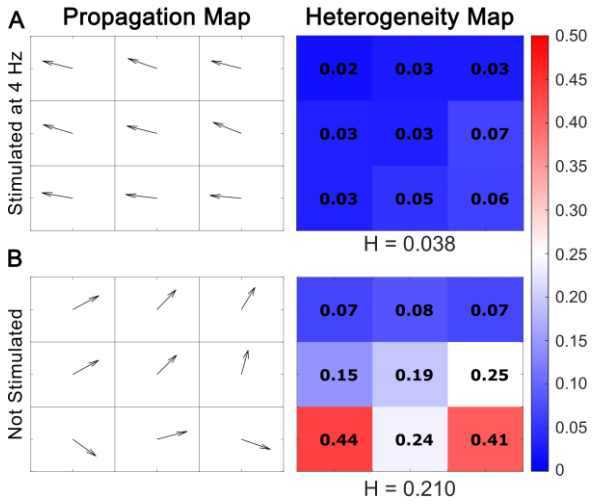

Figure 3. Examples of heterogeneity maps displaying the coefficients $v_{i,j}$ (see legend) of each clique and the global heterogeneity value *H*. A. Results for a recording stimulated at 4 Hz. On the left, the propagation vector map; right, the heterogeneity map. B. Idem for a recording without stimulation.

Fig. 4a. displays the distributions of all the *H* values obtained according to the stimulation type. When there is no stimulation, a mean value of 0.20±0.11 is obtained, but when stimulation occurs at 4 and 6 Hz, the *H* value drops to 0.06±0.02 for both groups.

The Receiver Operating Characteristic (ROC) was computed to compare the sensitivity and specificity of the binary classification system (basal/stimulated). The measure of a good classifier's performance in distinguishing between the two groups was quantified by the Area Under the Curve (AUC). With the resulting values of *H*, a ROC curve is obtained with an AUC of 0.996 and an optimal threshold value of 0.113. The application of this threshold produces the confusion matrix displayed in fig. 4b. The metrics for this confusion matrix are presented in Table 4c.

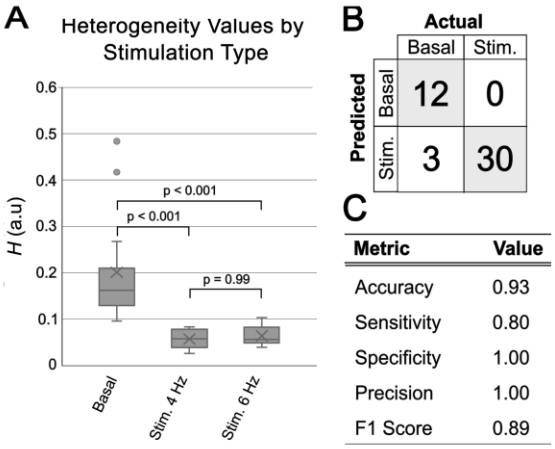

Metric	Value
Accuracy	0.93
Sensitivity	0.80
Specificity	1.00
Precision	1.00
F1 Score	0.89

Figure 4. A Box and whisker plot of the H values according to the type of stimulation. B. Confusion matrix for a threshold of 0.113. C. Table with the metrics derived from the confusion matrix.

5. Discussion

A metric to measure the disorganisation of cardiac electric propagation is proposed. The methodology is intrinsic to vector maps, allowing its adaptation to other catheter types by a simple tweaking of the parameters. The results demonstrate the discriminatory ability of the parameter, assigning higher values to heterogeneous maps (non-stimulated) and lower values to more homogeneous maps (stimulated). The statistical analysis confirmed this difference. The high AUC value indicates that the metric can accurately discriminate between stimulated and basal cases. Additionally, for the given threshold, the metric has achieved 100% accuracy in identifying recordings with stimulation, both at 4 and 6 Hz. No significant difference in heterogeneity was revealed when increasing the frequency of stimulation, with the vectors remaining aligned in both cases.

The main limitation of the study is the small number of vectors acquired by the *Advisor HD Grid* catheter. Despite this, the characterisation robustness facilitates the detection of local variations in heterogeneity that may be otherwise hidden for larger catheters. Other limitations include the unbalanced data set for the ROC analysis and the use of epicardial recordings. Future work should compare the metric to other state-of-the-art ones such as the Inhomogeneity Index [1], used broadly for quantifying inhomogeneities in cardiac conduction. It is also expected to evaluate the metric's performance using higher-density maps and larger sample sizes.

6. Conclusion

The success of the proposed heterogeneity metric is demonstrated through its ability to differentiate between stimulated and non-stimulated epicardial tissue, representing a promising step forward in the field of fibrotic or impaired tissue assessment.

Acknowledgments

We would like to thank GRELCA Lab for its support in performing the experiments. This project has been partially funded by the Ministry of Science and Innovation of the Government of Spain (PID2019-109547RB), and the Instituto de Salud Carlos III (CIBERCV CB16/11/00486). The animal experiments were conducted according to the guidelines approved by the ethical committee of the corresponding institutions.

References

[1] W. J. Lammers, M. J. Schalij, C. J. Kirchhof, and M. A. Allessie, 'Quantification of spatial inhomogeneity in conduction and initiation of reentrant atrial arrhythmias', American Journal of Physiology-Heart and Circulatory Physiology, vol. 259, no. 4, pp. H1254–H1263, Oct. 1990.

[2] G. W. Botteron and J. M. Smith, 'A technique for measurement of the extent of spatial organization of atrial activation during atrial fibrillation in the intact human heart', IEEE Trans Biomed Eng, vol. 42, no. 6, pp. 579–586, Jun. 1995.

[3] M.-N. Nguyen, H. Kiriazis, X.-M. Gao, and X.-J. Du, 'Cardiac Fibrosis and Arrhythmogenesis', *Comprehensive Physiology*, vol. 7, no. 3, pp. 1009–1049, 2017.

[4] K. Magtibay, A. Porta-Sánchez, S. K. Haldar, D. C. Deno, S. Massé, and K. Nanthakumar, 'Reinserting Physiology into Cardiac Mapping Using Omnipolar Electrograms', *Cardiac Electrophysiology Clinics*, vol. 11, no. 3, pp. 525–536, 2019.

[5] J. Riccio et al., 'Characterization of Atrial Propagation Patterns and Fibrotic Substrate With a Modified Omnipolar Electrogram Strategy in Multi-Electrode Arrays', *Front. Physiol.*, vol. 12, p. 674223, Sep. 2021.

[6] D. C. Deno, R. Balachandran, D. Morgan, F. Ahmad, S. Massé, and K. Nanthakumar, 'Orientation-Independent Catheter-Based Characterization of Myocardial Activation', IEEE Transactions on Biomedical Engineering, vol. 64, no. 5, pp. 1067–1077, 2017.

[7] L. J. van der Does and N. M. de Groot, 'Inhomogeneity and complexity in defining fractionated electrograms', *Heart Rhythm*, vol. 14, no. 4, pp. 616–624, 2017.

[8] A. Guill et al., 'QT Interval Heterogeneities Induced Through Local Epicardial Warming/Cooling. An Experimental Study', *Revista Española de Cardiología (English Edition*), vol. 67, no. 12, pp. 993–998, 2014.

[9] F. Castells et al., 'Performance assessment of electrode configurations for the estimation of omnipolar electrograms from high density arrays', *Computers in Biology and Medicine*, vol. 154, p. 106604, Mar. 2023.